Conformal Load-Bearing Antenna Structure for MIMO Applications

David L. Zeppettella [1] and Mohammod Ali [2]

[1] Air Force Research Laboratory, Dayton, OH 45433, USA
david.zeppettella@us.af.mil

[2] Department of Electrical Engineering, University of South Carolina, Columbia, SC 29208, USA
alimo@engr.sc.edu

Abstract ─ A broadband, airfoil-integrated, VHF antenna is introduced for conformal load-bearing structures (CLAS) applications. A two-layer antenna is developed and the effects of integration with a composite sandwich structure are investigated. A prototype structure is fabricated that exceeds an octave of measured impedance bandwidth and simulated gain and pattern bandwidth. Envelope correlation coefficient (ECC) and simulated radiation patterns are used to gauge feasibility of the structure for use in a MIMO application on a twin-tail drone.

Index Terms ─ CLAS, multifunctional structure, structural antenna.

I. INTRODUCTION

While the use of unmanned air vehicles (UAV) has traditionally been restricted to military operations, a number of private sector firms have recently announced plans to provide some type of commercial service that involves the use of a UAV. Applications such as package delivery and providing internet access in remote areas have been proposed. Although the concept of operations and type of service being provided may vary, one requirement common to all applications is the need for wireless communication systems and antennas on-board the aircraft. One specific application that has drawn significant interest is Cognitive Radio [1-2] communication where spectrum allocated for other applications but not in use at a particular instant can be used by another communication system. For example, consider television broadcast channels. If some of the channels are not used, some time-opportunistic sensing and leveraging could allow communication services through those channels. Sensing and reuse is the key, and thus broadband antennas or reconfigurable antennas will play a significant role.

The focus of the present paper is VHF communication, namely 90 MHz and higher. The goal is to obtain as much bandwidth as possible without sacrificing pattern and gain. Traditional broadband antenna solutions such as resistively matched antennas can provide broad bandwidths but suffer from very low gain [3]. Recent works on broadband matching of electrically small antennas using active circuits include the application of non-Foster active circuits [4-9]. The possibility of using non-Foster circuits to increase the bandwidths of a dipole [4], a monopole [5], a dipole [6], a loop and a broadband planar dipole [7] and a VHF monopole [8] antenna were studied. Although these methods provide useful performance improvements they are typically geared towards receiving application. Furthermore, they are complicated, and costly.

Given that many modern small and mid-sized UAVs are either fully or partially made of dielectric materials such as fiberglass or Kevlar composites, a new class of antennas that are integral to the mechanical structure of the UAV can be realized to provide superior performance characteristics. Such dual purpose structures have been termed generally as multi-function structures, and more specifically as Conformal Load-bearing Antenna Structures (CLAS) [10-13]. The key tenet of the CLAS concept is that a much larger antenna volume can be obtained by leveraging the outer surface area and structure of an air vehicle to implement large antennas or arrays, ultimately leading to increased effective aperture. Thus, from an RF perspective, this approach enables more efficient and broadband antennas. From an aircraft perspective, CLAS technology has minimal impact on vehicle weight and no impact on aerodynamic drag, unlike externally mounted blade antennas and pods that protrude into the airstream. However, CLAS design is a multi-disciplinary undertaking that must consider the desired RF performance, mechanical loading requirements, and properties of structural composite materials. Typically, a subcomponent of the UAV, such as the fuselage or a wing, is selected to be designed as a multi-function structure. To enable operation as an antenna, conductors of the proper thickness must be included with the composite structural materials, and such conductors need to be deposited or bonded to all other materials comprising the structure in a manner that does not

degrade mechanical performance.

As mentioned, the focus of this paper is to design and develop a broadband CLAS VHF antenna structure. The preliminary feasibility study of a VHF antenna for airfoil integration was presented in our conference paper [14] which included the design using copper foil and foam and parametric simulations of the antenna using FEKO. The work presented in this paper goes far beyond that. The objectives are to investigate if a broadband VHF CLAS assembly can be designed with significant bandwidth and nearly omni-directional pattern looking downward, study the effect of structural materials on bandwidth through Characteristic Mode Analysis, and validate simulated results through measurement of prototype structures. Finally, also investigate the potential for such CLAS components to be used in a MIMO configuration on a twin-tail UAV by computing the correlation coefficients and the patterns.

II. ANTENNA CONFIGURATION

As mentioned, the original geometry can be found in our previous paper [14]. The idea is to integrate the antenna into a composite airfoil such as shown in Fig. 1, and a cross-sectional schematic of the initial integration concept can be seen in Fig. 2. As seen, the antenna consists of two traces, Antenna Trace 1 and Antenna Trace 2, that are included at the interfaces of two of the four layers of dielectric materials making up the structure. Antenna Trace 1 is inserted between the lower skin and the first foam layer. Antenna Trace 2 is inserted between the two foam layers in the core of the structure. The Lower and Upper skins are made from dielectric materials commonly used in the fabrication of composite aircraft structures, e.g., fiberglass. In a practical specimen the antenna will be excited using a coaxial cable. For simplicity, the illustration in Fig. 2 shows a sinusoidal excitation as the feed. The separation between the Lower and Upper skins and the thicknesses of the different layers of dielectric materials are variables and depend on both the expected mechanical load and the desired antenna performance.
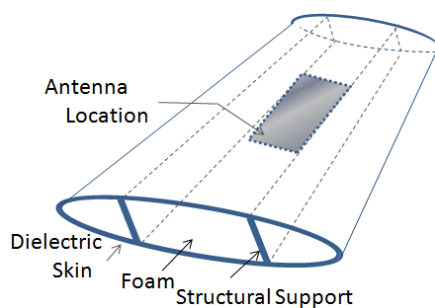

Fig. 1. Airfoil geometry and antenna location.

Initially the antenna design started without the presence of any dielectric materials to understand the

dependency of the antenna performance on conductive material design variables. Subsequently the dielectric materials were added on and adjustments for tuning were made. The design started with two rectangular conducting traces. The size of the larger conducting trace, e.g., Antenna Trace 1 is ultimately constrained by the size of the air foil, with more space being available span-wise than chord-wise, and a limit of 76 cm by 62 cm was considered. The thickness of conductive material considered was127 μm. The initial length of the smaller conducting trace, e.g., Antenna Trace 2 was determined by assuming that the antenna is a quarter wave monopole sized to operate at the center of the band of interest (150 MHz). Thus the initial length was determined to be 50 cm; however, the structural composite materials into which the antenna will eventually be placed have a dielectric loading effect. To compensate for this, the initial length for the small rectangle was shortened to 40 cm, which corresponds to an operational frequency of 187.5 MHz in free space.

Antenna design was targeted towards obtaining as much bandwidth as possible within these and other dimensional constraints. The height between Antenna Traces 1 and 2 was varied and many other parameters were varied to arrive at an optimum design. These studies were conducted using FEKO. The design progress summary is illustrated in Fig. 3. It was found that a spacing of 3.5 cm resulted in good return loss bandwidth. Detail descriptions on the design evolution are available in [14]. Several key adjustments were made to the initial starting design, namely: (1) Two stubs and a slot were added to Antenna Trace 1, and (2) Antenna Trace 2 was moved slightly towards the slot from the outer edge to create an overhang.

The overhang feature was introduced to improve the impedance match by creating and controlling the equivalent shunt capacitance resulting from Antenna Trace 2. Table 1 shows the final dimensions.

This antenna serves as the baseline antenna for this paper and will provide a basis for comparison during the process of converting the initial concept into a CLAS design. Table 2 lists the antennas that will be discussed and gives a brief description of each. Antenna C indicates the design when integrated within composite materials (details given in Section III. B), while Antennas D and E each represent pairs of antennas for MIMO operation (details given in Section III. E).
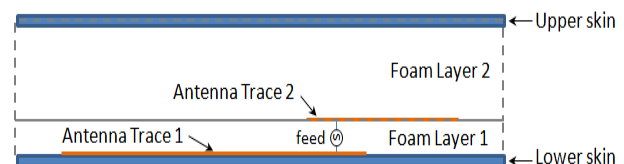

Fig. 2. Antenna and materials layout, cross-sectional view.

Table 1: Dimensions of the proposed antenna

Parameter	cm	Parameter	cm
W	62	g	12
L	76	h	8
c	40	1	14
d	22	w	6
e	3.5	i	8
s	58		

Table 2: List of antennas

Name	Description
Antenna A	Copper sheet and air
Antenna B	Expanded metal and foam
Antenna C	Composite sandwich
Antenna D	Dual parallel tail
Antenna E	Dual canted tail
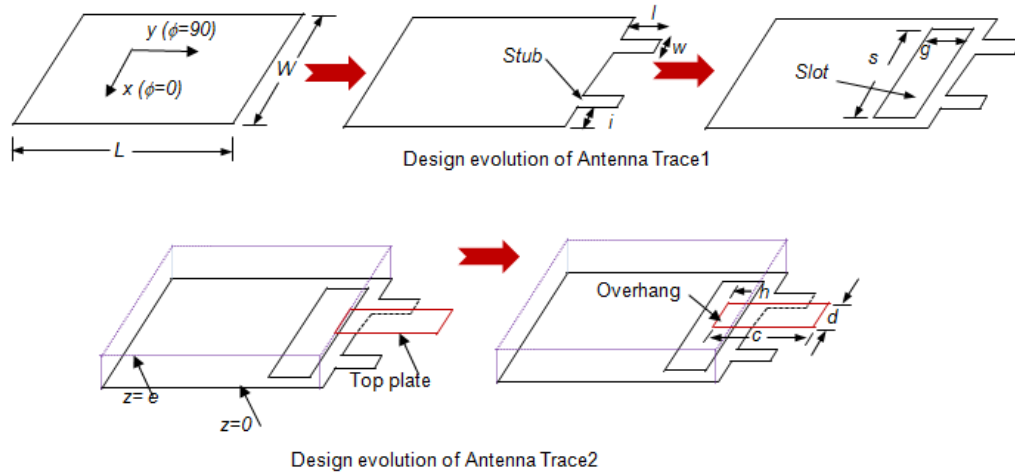
Fig. 3. Antenna design evolution.

III. RESULTS

A. Antenna A – No dielectric materials
Simulation results (bandwidth and pattern)

Simulated S_{11} results of Antenna A, with dimensions noted in Table 1, are shown in Fig. 4. As the plot shows, the S_{11} is below -10 dB from approximately 96 MHz to 241 MHz. Thus a 2.5:1 bandwidth is achieved.
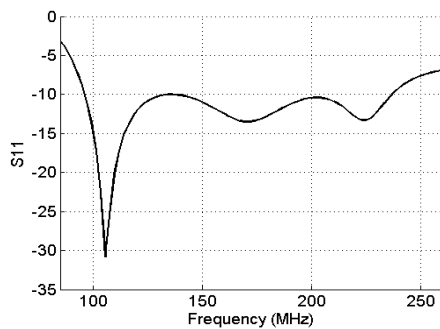

Fig. 4. Simulated S_{11} for Antenna A.

Figure 5 shows simulated radiation patterns for the three principal planes at 97 MHz and 240 MHz. The patterns are consistent over much of the frequency band with some distortion present at the upper end. It should be noted that although the θ=90 degree pattern at 240 MHz shows a null along what would be the azimuth for an aircraft, there are still lobes directed both above and below this plane. Thus, it is reasonable to expect that RF systems utilizing the antenna would continue to function across the band, albeit with some degradation at the higher frequencies.

Characteristic mode understanding

To understand the return loss bandwidth of the antenna from a Characteristic Mode (CM) theory point of view, CM simulations were conducted using FEKO. The objective was to determine the different modes that may have resulted from the antenna of Fig. 3 and their role in determining the overall antenna operating bandwidth.

CM analysis has been applied by other researchers to understand antenna modes, modal significance, and bandwidths from a CM point of view [15-17].

CM theory was introduced in the late 1960's by Garbacz who proposed that characteristic currents could be determined through analysis of the scattering matrix [18]. These characteristic currents are real surface currents on a conducting body that depend only on the geometry of the body and are independent of any external excitation. Later, Harrington and Mautz expanded upon the theory by proposing that the impedance matrix could also be used for this purpose [19, 20] through solution of the weighted eigenvalue equation:

$$[X]\overrightarrow{J_n} = \lambda_n [R]\overrightarrow{J_n}, \quad (1)$$

where R and X represent the real and imaginary part of the impedance matrix of the conducting body, λ_n are the

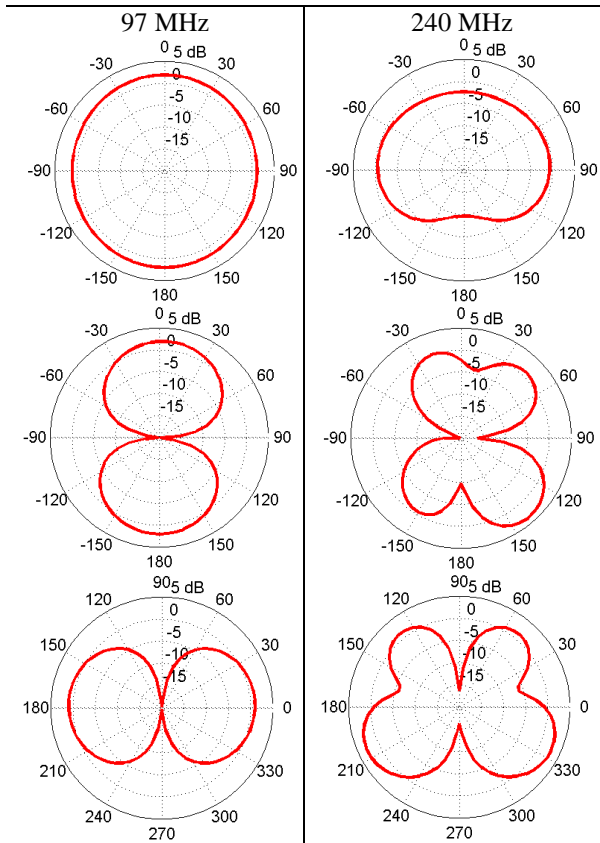eigenvalues, and $\overrightarrow{J_n}$ are the characteristic currents.

Fig. 5. Radiation patterns at $\varphi = 0$, $\varphi = 90$, and $\theta = 90$ planes.

In general, the magnitude of the eigenvalue, $|\lambda_n|$, is a figure of merit that indicates how well a given mode radiates. Modes for which $|\lambda_n|$ is small are the most effective radiators, while large values of $|\lambda_n|$ indicate that a mode is a poor radiator [21]. Resonance is indicated when the value of λ_n is zero.

One use of the eigenvalue is to calculate the so-called modal significance, as given by (2):

$$MS = \left| \frac{1}{1 + j\lambda_n} \right|. \qquad (2)$$

Modal significance is essentially an alternative representation for eigenvalues and it represents the normalized amplitudes of the eigencurrents [22]. In (2) it is easily observed that modal significance takes on a value of one in the case of resonance ($\lambda_n = 0$), and goes to zero for large values of λ_n [23]. A useful application of modal significance is to determine which characteristic modes are significant in terms of contributing to radiated power. A mode is considered significant when $MS > \dfrac{1}{\sqrt{2}}$

while the case of $MS < \dfrac{1}{\sqrt{2}}$ indicates a non-significant mode [24].

A modal significance plot computed using FEKO for Antenna A is shown in Fig. 6. The dashed line in the figure indicates a modal significance of 0.7; thus it is easily seen that modes 1, 2, and 4 are significant while mode 3 is non-resonant and does not contribute to radiated power over the frequency band of interest. Furthermore, considering the modal half-power bandwidth, defined as:

$$BW_n = \frac{f_u - f_l}{f_r}, \qquad (3)$$

where f_u and f_l are the upper and lower frequencies at which $MS = 0.7$, f_r is the resonant frequency ($MS = 1$), and the subscript n denotes the nth mode, the bandwidth of mode 2 is found to be 51%, mode 4 has a bandwidth of 29%, and mode 1 has a bandwidth of 19%. One interesting aspect of the modal significance plot is that there are no significant modes between about 115 and 150 MHz (Fig. 6); yet the S_{11} plot shown in Fig. 4 shows the match is good over this frequency band. It would initially seem that there should be another dominant mode over this frequency range. The concept of modal interaction described in [17] can be used to explain this discrepancy which states that modal interactions between the modes essentially create a matching circuit that provides a good S11 match even in the absence of $MS \geq 0.7$.
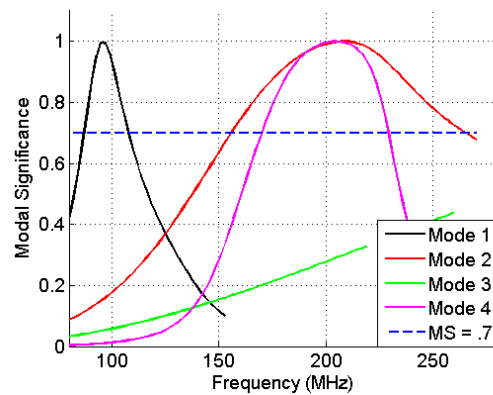

Fig. 6. Modal significance for Antenna A.

The current distribution on the antenna was also studied using FEKO. Figure 7 shows the current distribution at three different points within the frequency band over which S_{11} is below -10 dB. It is apparent that the stubs become more active and the current is more concentrated toward the edges of Antenna Trace 1 at higher frequencies.
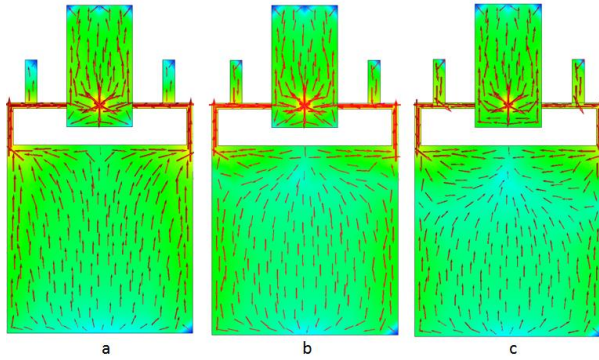
Fig. 7. Current distribution for a) 96 MHz, b) 142 MHz, and c) 238 MHz.

Experimental results

A prototype of Antenna A was fabricated using the dimensions detailed in Table 1. The antenna traces were precision cut from a roll of copper sheeting with a width of 91 cm (3 ft) and a thickness of 127 μm (5 mil) to enable a continuous conductive surface. Two 3.5 cm thick pieces of Rohacell foam were cut from a large block to serve as a spacer between the traces. An L-shaped piece of polyethylene was attached to the sides of the foam sheets with plastic screws to add mechanical stiffness. The antenna traces were then positioned with proper orientation to each other on opposite sides of the foam spacer and secured in place with masking tape. A photo of the prototype with the slotted trace visible is shown in Fig. 8 (a).
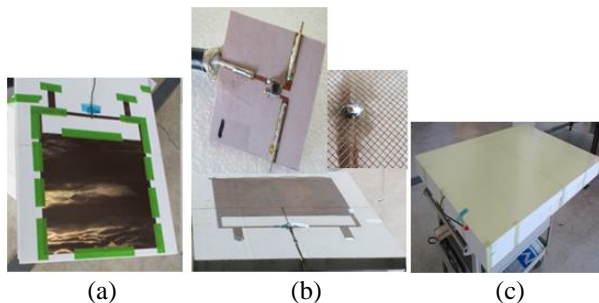

(a) (b) (c)

Fig. 8. (a) Antenna A, (b) Antenna B with insets showing feed board and nature of mesh, and (c) Antenna C.
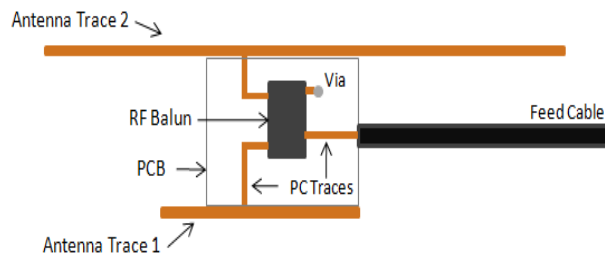

Fig. 9. Cross sectional view of feed showing the orientation of the balun PCB.

At the feed point, a section of foam was removed between the traces, and a PCB containing an RF balun from RF Micro Devices (part no. RFXF9503) was positioned between the upper and lower traces. The PCB, which is shown on the upper right of Fig. 8 (b), had a 50 ohm microstrip line at the input and two traces on the output side to attach wires for connection to the antenna traces. A coaxial cable was soldered directly to the PCB input, and the other end of the cable was terminated with an SMA connector. The PCB is 3.5 cm wide, and is installed vertically between the two copper layers to minimize wire lead length. Wires with a diameter of 0.9 mm were soldered to each PCB output terminal, and the wires were in turn soldered to the copper sheets at the feed point. Figure 9 is an illustration of the feed assembly.

Upon completing assembly of the antenna, S_{11} measurements were taken. Given the VHF operating range of the antenna, the measurement was made in a large aircraft hangar with a ceiling height of approximately 80 feet. The antenna was placed on top of two large foam blocks at a height of approximately 1.5 m above the floor and secured with tape. An Agilent E5071CVNA was placed on a cart and positioned next to the foam blocks with the connection between the VNA cable and antenna feed cable secured to the top of the foam block with tape.

Simulated and measured S_{11} data are compared in Fig. 10. In terms of bandwidth within S_{11} below -10 dB the two results are in good agreement. The measured S_{11} is below -10 dB from 93 MHz to 230 MHz, for a bandwidth ratio of 2.47:1. This agrees well with the simulated -10 dB bandwidth of 96 to 241MHz (2.5:1 ratio). The main discrepancy is at the upper end of the frequency band. This could be due to a slight difference in the feed between the model and the prototype antenna. A larger diameter wire (5 mm) was used in the simulation than was available when the prototype was constructed, and the smaller 0.9 mm wire and thin PCB trace used to feed the prototype could have caused this reduction in the bandwidth.
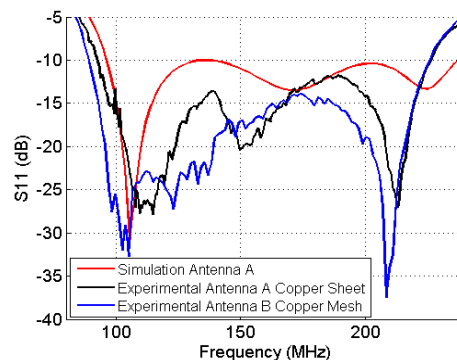

Fig. 10. Comparison of simulated and measured S_{11} of prototype antennas.

To move toward a more structural version of the antenna, Antenna B was constructed using expanded metal instead of the solid copper sheets. Solid copper cannot be used in structural composite applications because it is difficult to bond to a component, and, even if this were possible, it would represent a significant parasitic weight increase for the structure. Expanded metal is commonly used on composite aircraft for lightning strike protection, and it is essentially a metallic mesh that is produced by interweaving small diameter wires or stamping a mesh pattern from a solid conductive sheet. The porous nature of the mesh allows structural epoxy to flow through and bond the mesh to the surface of a composite part during curing. From a mechanical perspective, the mesh is easier to conform to complex shapes and contributes less parasitic weight than a solid sheet. A mesh material from Astroseal Products Mfg. Corp. having grid dimensions of 1 mm by 1.6 mm and a thickness of 130μm was used for the prototype antenna. Fig. 8 (b) shows Antenna B with Antenna Trace 1 visible. The nature of the mesh material can be seen in the close-up on the upper left, which shows the area around the feed. The S_{11} measurement was repeated, and the results are shown by the blue line in Fig. 10. It was found that Antenna B had a slightly higher bandwidth ratio (2.5:1) than Antenna A (2.47:1). This came about because Antenna A was inadvertently fabricated with 5 mm less vertical spacing between the upper and lower traces.

B. Structural integration effects
Simulation results (bandwidth and pattern)

As seen in Fig. 2, the proposed antenna would have to be integrated within a structural sandwich containing various dielectric materials. The effects of such integration were studied through simulations in FEKO. Initially the configuration shown in Fig. 11 was simulated. As seen, Antenna Trace 1 is in direct contact with the Lower skin. Antenna Trace 2 is much farther away from the Upper skin. The thickness of the Lower and Upper skins was 5 mm. Although it is recognized that some additional supporting mechanical structure would be required, this was not included in the initial simulations. It was also assumed that the airfoil would have a significant through-thickness dimension because only a large airfoil would be able to accommodate the 1.16 m by 0.62 m antenna.
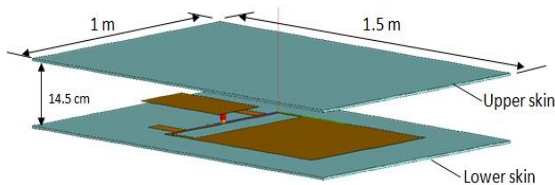

Fig. 11. Addition of dielectric sheets to represent a composite sandwich structure (Antenna C).
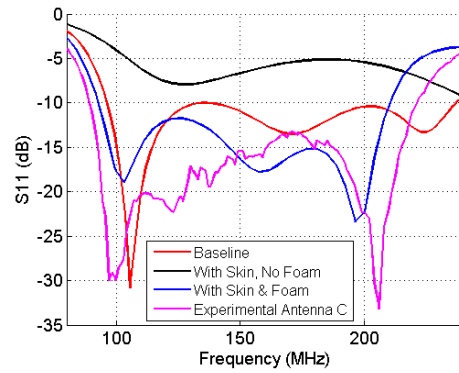

Fig. 12. Simulated S_{11} of antenna in the presence of dielectric skins. Cases with and without foam are shown.
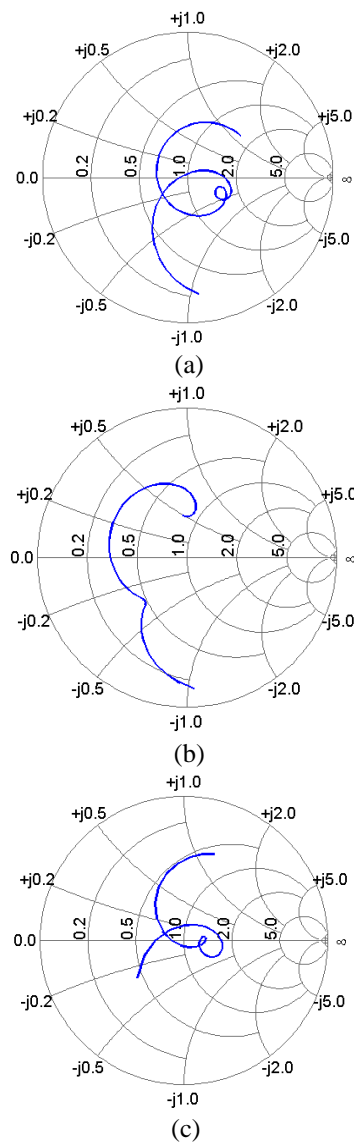

Fig. 13. Smith charts showing simulated data for: (a) baseline antenna (no dielectric), (b) fiberglass skin, no foam buffer, and (c) fiberglass with 5mm foam buffer.

The dielectric skin layers were modeled as 1.5 m by 1 m fiberglass composite sheets with $\varepsilon_r = 4.0$ and $\tan\delta = 0.01$. The foam was modeled as air because $\varepsilon_r = 1.08$ is typical for foam used in structural composites. Simulated S_{11} results for this pseudo-structural antenna are shown in Fig. 12 (black trace). Comparing that with the S_{11} response of the baseline antenna in free space without any dielectric (red trace), it is obvious that the presence of the dielectric skin materials has significantly degraded the antenna performance. To examine the variability in dielectric constant and its effect on antenna performance, a second simulation was performed by replacing the fiberglass skins with cyanate-ester/quartz ($\varepsilon_r = 3.25$, $\tan\delta = 0.006$). Interestingly, the results were the same as for fiberglass, suggesting that the problem was with the integration scheme itself as opposed to arising from material properties.
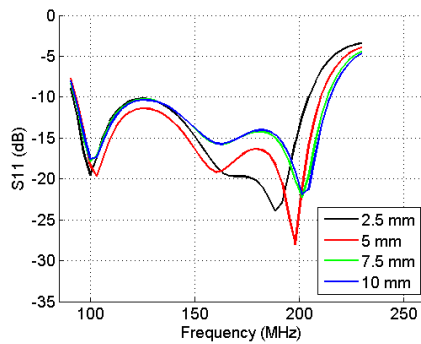

Fig. 14. Effect of foam buffer thickness on S_{11}.

The integration concept was reconsidered, and it was noted that the only major difference between the structural and non-structural antenna was that the lower dielectric sheet was in direct contact with the slotted conductive trace in the structural version. The dielectric sheet was moved down 5 mm (see Fig. 11) in the FEKO model to determine if the mere presence of dielectric material near the feed and slot area was affecting the input impedance of the antenna. This 5 mm of separation could be achieved in a composite structure by adding an additional foam layer between the lower sheet and the slotted trace.

As indicated by the blue line on the S_{11} plot of Fig. 12, a significant portion of the previously observed bandwidth was recovered through the inclusion of the foam buffer. The bandwidth ratio for the structural antenna is 2.26:1 with the reduction occurring at the high end of the operational band. It was also noted that the beginning of the operating band shifted downward slightly from 96 to 93 MHz.

Figure 13 shows the structural interaction discussed above on a Smith chart. Fig. 13 (a) is the baseline antenna in air, and Fig. 13 (b) shows the deleterious effect of the dielectric skin being in direct contact with

Antenna Trace 1. The Smith chart of Fig. 13 (c) shows that the inclusion of the foam buffer results in much improved performance that is similar to that observed for the baseline antenna.

The effect of the foam buffer thickness on S_{11} was investigated through additional simulations, and the resulting data are shown in Fig. 14. It was determined that a foam thickness greater than 5 mm resulted in slightly more bandwidth, while a thickness under 5 mm resulted in less bandwidth. The buffer thickness was ultimately left at 5 mm because it provided a slightly better match over most of the band and facilitated structural fabrication by making the antenna less intrusive into the structure. Simulated radiation pattern plots are shown in Fig. 15. Table 3 shows the peak gain at discrete points in the operating band for each of the dielectric materials that were studied.
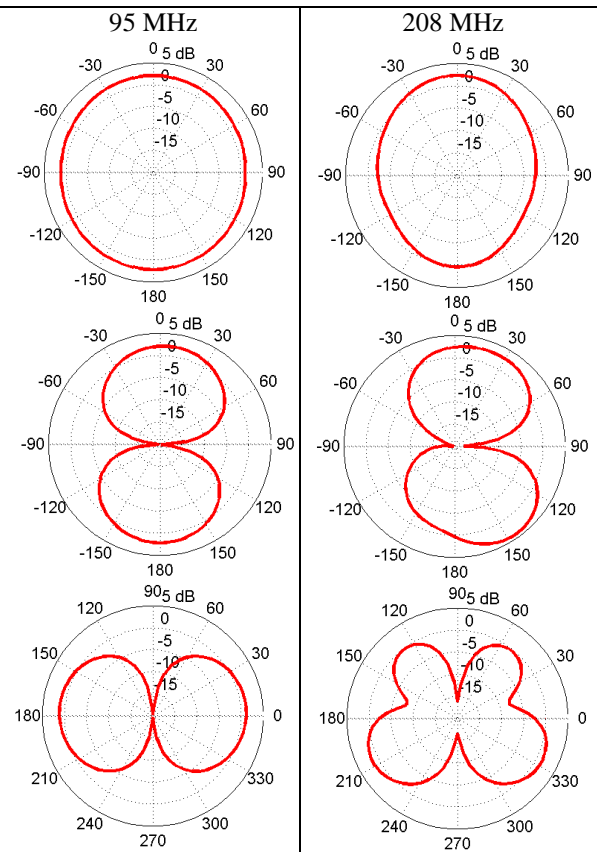

Fig. 15. Radiation patterns at $\varphi = 0$, $\varphi = 90$, and $\theta = 90$ planes.

Table 3: Comparison of simulated peak gain for different composite materials (dBi)

Dielectric	100 MHz	150 MHz	200 MHz
None	2.2	2.7	2.7
Cyanate-Ester Quartz	2.4	2.7	2.7
Fiberglass	2.3	2.6	2.4

From a comparison of Fig. 15 and Fig. 5, it is evident that the patterns in each of the principal planes at the lower end of the band are similar. Comparing the patterns at the upper end of the band in Fig. 15 to those in Fig. 5, it is seen that there is close agreement in the $\theta = 90$ degree plane, but some variation is found in the other planes. This is because the upper end of the band is 221 MHz in Fig. 15, whereas it is 240 MHz in Fig. 5.

Characteristic mode understanding

The CM analysis was repeated for the antenna integrated with the structural skin and in the presence of the foam. FEKO simulation results generated the modal significance plot shown in Fig. 16. In general, these results agree with the results seen in Fig. 6 for the non-structural antenna. However, two differences are noted. First, for the structural antenna with the skins and foam, all of the frequencies of the resonant modes have shifted lower. Second, modes 1, 2, and 4 have somewhat narrow bandwidths. Table 4 compares modal bandwidths calculated for Antennas A and C.
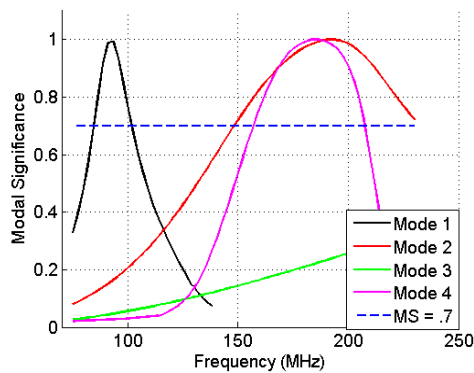

Fig. 16. Modal significance for structural antenna.

Table 4: Comparison of modal bandwidth for Antenna A and Antenna C

Mode	Bandwidth (MHz) (Antenna A)	Bandwidth (MHz) (Antenna C)
1	21.4	18.3
2	106.7	80.8
4	59.5	50.8

Experimental results of structurally integrated antenna

Upon completing the analysis of structural integration effects, Antenna C was constructed (see Fig. 8 (c)) using 2 mm thick fiberglass sheets instead of the 5 mm thick fiberglass and cyanate-ester quartz sheets used in the simulations. The thinner sheets were already on-hand, and this change saved the cost of purchasing commercial composite sheets or the supplies needed to manufacture custom composite panels, not to mention the labor cost and time associated with manufacturing. The expected impact of the thinner material was that

measured performance would be slightly better than for the thicker dielectric used in simulations. The measured S_{11} versus frequency for this antenna are shown in Fig. 12 using the magenta line. As seen, the operating bandwidth within -10 dB S_{11} is from 89 to 221 MHz. As expected, the measured performance of Antenna C was better than the simulation results (2.48:1 bandwidth ratio vs. 2.26:1), but it is evident in Fig. 10 that Antenna C has less bandwidth than Antenna B - which agrees with what was observed in simulations.

C. MIMO application

A common vehicle configuration for UAVs is the inverted V tail, in which the conventional horizontal and vertical stabilizers are replaced by two airfoils that are oriented downward at an angle from the horizontal. Such a structure could be used to implement a structural VHF antenna to enable an airborne MIMO capability. MIMO has been suggested as a means of increasing throughput for communications links [25-27] and improving radar performance [28].

To investigate the feasibility of this concept, two vertically oriented structural antennas (Antenna C) were used to approximate an aircraft having two parallel tails. This physical configuration is designated as Antenna D in Table 2. Because independent antennas are required for MIMO applications, the envelope correlation coefficient (ECC) was used to characterize the relative independence of the antennas. The ECC study was conducted by first using FEKO to calculate the S-parameters with the antennas being separated by distances of 1 m, 1.25 m, and 1.5 m. The resulting data was post-processed using MATLAB to calculate ECC for each case. Simulations indicated that the efficiency of the antenna is on the order of 98%, so accurate results for ECC can be expected through the use of S parameters as given by (4) [29]

$$ECC = \frac{|S_{11}^* S_{12} + S_{21}^* S_{22}|^2}{(1 - |S_{11}|^2 + |S_{21}|^2)(1 - |S_{21}|^2 + |S_{12}|^2)}. \quad (4)$$
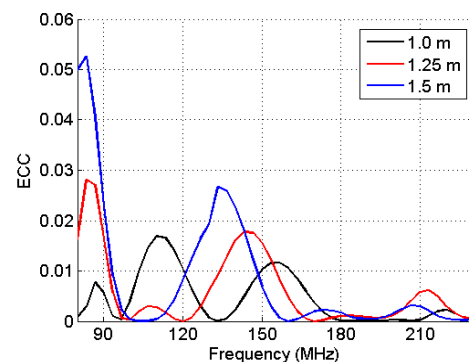

Fig. 17. ECC for vertical tails separated horizontally by 1.0, 1.25, and 1.5 m.

Figure 17 shows plots of ECC versus frequency for each separation distance over the band of interest. The data indicate that not only is ECC low for all separation distances, the case of 1 m separation results in the lowest overall ECC across the band. This result is encouraging because a 1 m separation distance is a reasonable value for tail separation on a twin tail UAV.
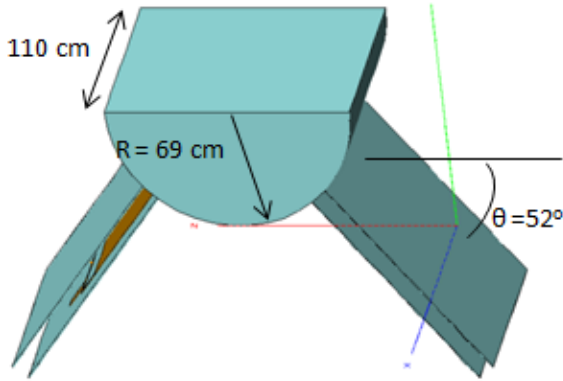

Fig. 18. FEKO model of an inverted V-tail UAV configuration.
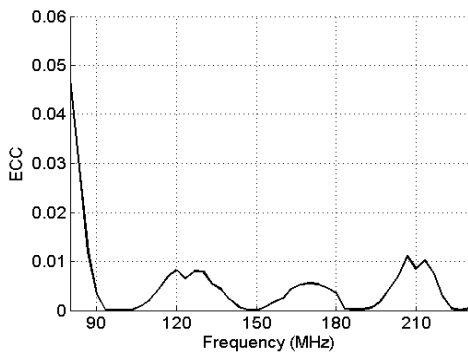

Fig. 19. ECC for the inverted V tail model.

Given the encouraging ECC results obtained with the parallel tail configuration, another study was conducted with the antennas canted at a 52 degree angle from the horizontal to represent antennas being integrated with inverted V tails. This configuration is designated as Antenna E, and is shown as a FEKO model in Fig. 18. The model also includes a section of fuselage with a radius of 69 cm and length of 110 cm. It was assumed that the fuselage is a cyanate-ester quartz composite with a thickness of 5 mm. The forward and aft sections of the fuselage are closed out with a 5 mm thick composite panel representing a bulkhead, although we note that the aft section would be partially open to accommodate a propeller shaft. The tails themselves are represented as Antenna C of Fig. 11 having the same dimensions with the exception that the spacing between the dielectric sheets was reduced to 10 cm.

The previously described process was used to calculate ECC based on (4) for the inverted V tail model, and the results are shown in Fig. 19. A comparison of Figs. 19 and 17, shows that the inverted V tail configuration achieves a lower ECC than was realized with any of the parallel tail configurations previously studied.
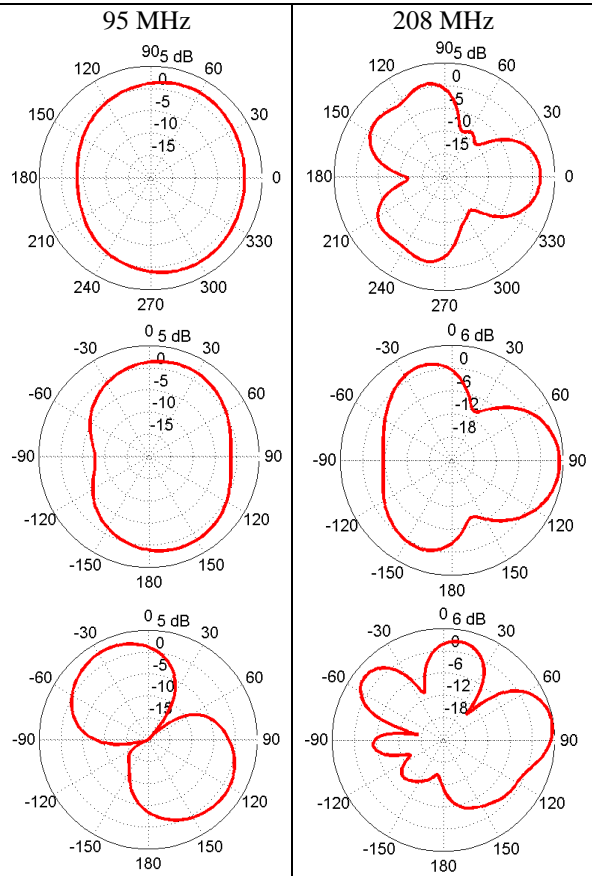

Fig. 20. Simulated radiation patterns for aircraft azimuth, pitch, and roll planes.

Simulated radiation patterns for the inverted V tail concept are shown in Fig. 20. The simulations were conducted with one antenna excited and the other terminated with a 50 ohm load. The patterns of each antenna were found to be nearly identical except for the orientation in the roll plane being canted at +/- 52 degrees as would be expected because this is the orientation of the antenna structure. The plots at the low end of the band in Fig. 20 show good symmetry with slightly more gain in the forward direction than aft (Fig. 20). At the upper end of the band in Figs. 20 (d-f), the patterns become more directional with energy being directed forward and outboard. While the null directed to the aft at the upper end of the frequency band could be undesirable in some applications, the independent

patterns combined with low ECC value across the band indicate the use of tail-integrated antennas for a MIMO is feasible.

IV. CONCLUSION

The study, design, and fabrication of a broadband VHF antenna for integration into a composite airfoil are presented. It is demonstrated that a broadband antenna operating from 89-221 MHz can be incorporated into composite structures. Simulation and experimental results clearly show that such antennas can be built using structural composite materials, such as cyanate-ester/quartz, Rohacell foam and conductive mesh with appropriate thicknesses commensurate with the frequency band of operation. The need for a foam buffer layer in between the antenna trace and the dielectric skin is demonstrated and the thickness of such a layer is optimized through simulations. Characteristic Mode (CM) analyses are performed to further understand and elucidate the bandwidth of the antenna as function of its modes and modal significance. The CM analyses was conducted in two ways with the first being a single sweep from 80 to 235 MHz, and the second being a segmented approach consisting of three separate simulations over subsets of the operational band. The latter approach was adopted because FEKO indicated that tracking errors occurred during the single sweep analysis. The details on the CM simulations of the antenna are available in [30].

The CM analyses for most of the antennas clearly delineate the individual modes and the modal interactions by means of which the antenna achieves broadband performance. The CM simulations also demonstrate the effects of the composite material loading on antenna operating frequency and bandwidth. Multiple antenna prototypes were built and tested. The final one was a sandwich structure consisting of cyanate-ester/quartz skins, Rohacell foam, and copper mesh. Experimental results on this antenna demonstrate antenna bandwidth from 89-221 MHz. Simulated radiation patterns show good coverage with a gain between 2 and 3 dBi across the band. The proposed sandwich structure antenna was also studied for possible MIMO application under an inverted V tail UAV configuration. The two antennas in that configuration clearly show excellent performance based on their ECC and simulated radiation patterns.

ACKNOWLEDGMENT

REFERENCES

[1] J. Mitola and G. Q. Maguire, "Cognitive radio: making software radios more personal," *IEEE Personal Communications*, vol. 6, no. 4, pp. 13-18, Aug. 1999.

[2] Y. Tawk, S. K. Jayaweera, C. G. Christodoulou, and J. Costantine, "A comparison between different cognitive radio antenna systems," *International Symposium on Intelligent Signal Processing and Communication Systems (ISPACS)*, pp. 1-5, Dec. 2011.

[3] C. J. Leat, "Resistively loaded helical antennas for ground-penetrating radar,'' *IEE Proc. – Micro-waves, Antennas, and Propagation*, pp. 204-210, Jan. 2003.

[4] S. E. Sussman-Fort and R. M. Rudish, "Non-Foster impedance matching of electrically-small antennas," *IEEE Trans. Antennas Propagat.*, vol. 57, no. 8, pp. 2230-2241, Aug. 2009.

[5] K. S. Song, *Non-Foster Impedance Matching and Loading Networks for Electrically Small Antennas*, Ph.D. Dissertation, The Ohio State University, 2011.

[6] M. Hirvonen, A. Hujanen, J. Holmberg, and J. C. E. Sten, "Bandwidth limitations of dipoles matched with non-Foster impedances," *IEEE Antennas Propagat., Soc. Euro. Conf.*, pp. 1-5, Nov. 2007.

[7] S. Koulouridis and J. L. Volakis, "Non-Foster circuits for small broadband antennas," *IEEE Antennas Propagat. Soc. Intl. Symp.*, Charleston, SC, pp. 1-4, June 2009

[8] C. R. White, J. S. Colburn, and R. G. Nagele, "A non-Foster VHF monopole antenna," *IEEE Antennas Wireless Propagat. Lett.*, vol. 11, pp. 584-587, 2012.

[9] M. N. Alam, R. Dougal, and M. Ali, "Electrically small broadband VHF/UHF planar antenna matched using a non-Foster circuit," *Microwave Optical Technol. Lett.*, vol. 55, pp. 2494-2497, Oct. 2013.

[10] J. Tuss, A. Lockyer, K. Alt, F. Uldrich, R. Kinslow, J. Kudva, and A. Goetz, "Conformal load bearing antenna structure," *in Proc. 37th AIAA Structural Dynamics and Materials Conf.*, pp. 836-843, 1996.

[11] P. J. Callus, "Novel Concepts for Conformal Load-bearing Antenna Structure," Defense Technical Information Center, Fort Belvoir, VA, 2007.

[12] D. Banks, M. Berden. W. Baron, and J. Tenbarge, "Structurally integrated X-band array develop-ment," *Multifunctional Structures /Integration of Sensors and Antennas*, Neuilly-sur-Seine, France: RTO, Meeting Proceedings RTO-MP-AVT-141, paper 17, pp. 17-1-17-12, 2006.

[13] N. Bishop, J. Miller, D. Zeppettella, W. Baron, J. Tuss, and M. Ali, "A broadband high-gain bi-layer

LPDA for UHF conformal load-bearing antenna structures (CLAS) applications," *IEEE Trans. Antennas Propagat.*, pp. 2359-2364, May 2015.

[14] D. Zeppettella and M. Ali, "VHF antenna for airfoil structural integration," *IEEE Antennas and Propagation Society International Symposium*, June 26 – July 1, 2016. DOI:10.1109/APS.2016.7696637

[15] B. Strojny and R. Rojas, "Characteristic mode analysis of electrically large conformal bifilar helical antenna," *Proceedings of the Fourth European Conference on Antennas and Propagation (EuCAP)*, Apr. 2010.

[16] B. Raines and R. Rojas, "Design of frequency reconfigurable antennas using the theory of network characteristic modes," *IEEE Trans. Antennas Propagat.*, pp. 3106-3113, Oct. 2010.

[17] J. Adams and J. Bernhard, "A modal approach to tuning and bandwidth enhancement of an electrically small antenna," *IEEE Trans. Antennas Propagat.*, pp. 1085-1092, Apr. 2011.

[18] R. J. Garbacz, *A Generalized Expansion for Radiated and Scattered Fields*, Ph.D. dissertation, Dept. of Electrical Engineering, The Ohio State University, Columbus, OH, 1968.

[19] R. F. Harrington and J. R. Mautz, "Theory of characteristic modes for conducting bodies," *IEEE Trans. Antennas Propagat.*, vol. AP-19, no. 5, pp. 622-628, Sept. 1971.

[20] R. F. Harrington and J. R. Mautz, "Computation of characteristic modes for sonducting bodies," *IEEE Trans. Antennas Propagat.*, vol. AP-19, no. 5, pp. 629-639, Sep. 1971.

[21] E. Newman, "Small antenna location synthesis using characteristic modes," *IEEE Trans. Antennas Propagat.*, vol. 27, no. 4. pp. 530-531, July 1979.

[22] B. A. Austin and K. P. Murray, "The application of characteristic-mode techniques to vehicle-mounted NVIS antennas," *IEEE Trans. Antennas Propagat.*, vol. 40, no. 1, pp. 7-21, Feb. 1998.

[23] W. Strydom and M. Botha, "Investigating antenna radiation properties with characteristic mode analysis," *AFRICON, 2013*, Mar. 6, 2014, DOI:10.1109/AFRICON.2013.6757604

[24] Y. Chen and C. Wang, *Characteristic Modes: Theory and Applications in Antenna Engineering*. John Wiley & Sons, Inc., Hoboken, New Jersey, 2015.

[25] D. Reith, C. Heller, D. Blaschke, and G. Aschield, "Line-of-sight MIMO in aircraft-to-aircraft data links," *IEEE/AIAA 33rd Digital Avionics Systems Conference (DASC)*, Dec. 11, 2014, DOI:10.1109/DASC.2014.6979437

[26] C. Zhang, K. Pang, and L. Ma, "Interpolated airborne MIMO antenna array," *IEEE Antennas Wireless Propagat. Lett.*, vol. 14, pp. 72-75, Sep.

[27] B. Holter, J. Hakegard, and T. Myrvoll, "On the use of MIMO in aeronautical communications," *Proc. 2nd ENRI International Workshop on ATM/CNS (EIWAC2010)*, Tokyo, Japan, 2010. SINTEF S17195.

[28] A. Flattie, "Performance evaluation of MIMO cooperative radar by considering high altitude aeronautical platforms," *International Conference on challenges in IT, Engineering and Technology (ICCIET2014)*, Phuket (Thailand), July 17-18, 2014. http://dx.doi.org/10.15242/IIE.E0714069

[29] C. Votis, G. Tatsis, and P. Kostarakis, "Envelope correlation parameter measurements in a MIMO antenna array configuration," *Int. J. Communications, Network and System Sciences*, 3, 350-354, 2010. doi:10.4236/ijcns.2010.34044. Published Online April 2010. http://www.SciRP.org/journal/ijcns/

[30] D. Zeppettella, *Multifunction Radio Frequency Composite Structures*, Ph.D. Dissertation, University of South Carolina, Columbia, SC, 2018.

David Zeppettella is an Electronics Engineer at the Air Force Research Laboratory where he leads research on multifunction structures. His research focuses on dual-purpose composite structures for structural state sensing and RF applications. He received his Ph.D. degree in Electrical Engineering from the University of South Carolina in 2018. Previously he received his M.S. degree in Electrical Engineering from The University of Dayton and his B.E. degree also in Electrical Engineering from Youngstown State University. Zeppettella has 19 years of engineering and R&D experience.

Mohammod Ali (M'93–SM'03) received the B.Sc. degree in Electrical and Electronic Engineering from the Bangladesh University of Engineering and Technology, Dhaka, in 1987 and the M.A.Sc. and Ph.D. degrees, both in Electrical Engineering, from the University of Victoria, Victoria, BC, Canada, in 1994 and 1997, respectively. Since August 2001, he has been with the Department of Electrical Engineering, University of South Carolina at Columbia where currently he is a Professor. He is the author/coauthor of over 180 publications and 9 US patents.